



Long bubbles in tubes filled with viscoplastic fluid



M. Jalaal^a, N.J. Balmforth^{b,*}

^a Department of Mechanical Engineering, University of British Columbia, Vancouver, BC, V6T 1Z4, Canada

^b Department of Mathematics, University of British Columbia, Vancouver, BC, V6T 1Z2, Canada

ARTICLE INFO

Article history:

Received 8 March 2016

Revised 27 May 2016

Accepted 8 June 2016

Available online 14 June 2016

Keywords:

Bubbles

Yield stress

Surface tension

ABSTRACT

An analysis is presented of the thin viscoplastic film coating the wall of a slot or tube as a long bubble is displaced down the conduit by ambient fluid flow (the viscoplastic version of a classical viscous problem studied by Bretherton). Lubrication theory is used to analyse the limit of low Capillary number and examine primarily the effect of a yield stress. The predictions are compared with the results of numerical simulations with the open source code Gerris.

© 2016 Elsevier B.V. All rights reserved.

1. Introduction

In a seminal paper in interfacial fluid mechanics in 1961, Bretherton [1] considered how a bubble contained in two-dimensional slot or axisymmetrical tube would be displaced down the length of that conduit by an ambient viscous fluid flow. Bretherton used lubrication theory, which applies when the bubble is long in comparison to its width or radius and the fluid films buffering the bubble from the walls are relatively thin. In the limit of small Capillary number (relatively strong surface tension) Bretherton demonstrated how the speed of the bubble was controlled by the thin fluid films, and provided the relation,

$$h_{\infty} \sim 1.34 R C^{2/3}, \quad (1)$$

where h_{∞} is the film thickness over the main bulk of the bubble, R is the slot half-thickness or tube radius and $C = \mu U / \sigma$ is the Capillary number, defined in terms of fluid viscosity μ , bubble speed U and interfacial tension σ . Bretherton's analysis, which is closely connected to the classical Landau-Levich theory for the draw-out of a film from a fluid bath by a plate [2], was subsequently extended to higher Capillary numbers by numerical simulations (e.g. [3,4]) and generalized to a number of generalized Newtonian and viscoelastic fluids [5–9].

The goal of the current article is to provide a short discussion of the viscoplastic version of Bretherton's problem. In particular, we focus on how a yield stress affects the relation between the residual film thickness and Capillary number. For the task, we use lubrication theory to furnish asymptotic solutions in the limit of

small Capillary number. We compare the predictions with numerical simulations using the open source code Gerris. That package cannot properly deal with a yield stress; instead, we regularize the constitutive model and use a bi-viscous law in the computations.

Previous computations and experiments for the propagation of bubbles down tubes filled with flowing viscoplastic fluid have been given by [10–13]. The existing computations deal with relatively large Capillary number, outside of the regime of validity of Bretherton's lubrication-style theory, and so there is minimal overlap between our results and these previous studies. Also relevant are experiments on the viscoplastic Landau-Levich problem [14,15] and the work of [16] on the steady motion of viscoplastic plugs down conduits representing idealized airways. A variety of other interfacial flow problems involving bubbles in viscoplastic fluids, of indirect relevance to the present work, are reviewed by [17].

2. Formulation

2.1. Governing equations

Consider a bubble in a slot or tube filled with Herschel-Bulkley fluid. The fluid flows down the conduit transporting the bubble at a speed that differs from the mean fluid speed. The arrangement is assumed symmetric about the midplane or centerline. Conservation of mass and momentum for the velocity field \mathbf{u} , pressure p and deviatoric stress $\boldsymbol{\tau}$ of an incompressible fluid take the form,

$$\nabla \cdot \mathbf{u} = 0, \quad (2)$$

$$\rho \left[\frac{\partial \mathbf{u}}{\partial t} + (\mathbf{u} \cdot \nabla) \mathbf{u} \right] = -\nabla p + \nabla \cdot \boldsymbol{\tau}, \quad (3)$$

* Corresponding author.

E-mail addresses: njb@math.ubc.ca, nbalmfor@eos.ubc.ca (N.J. Balmforth).

Here, ρ denotes fluid density and we adopt the Herschel-Bulkley law to relate the deviatoric stress tensor $\boldsymbol{\tau}$ to the deformation rates:

$$\begin{cases} \dot{\boldsymbol{\gamma}} = \mathbf{0}, & \tau < \tau_Y, \\ \boldsymbol{\tau} = \left(K\dot{\boldsymbol{\gamma}}^{n-1} + \frac{\tau_Y}{\dot{\boldsymbol{\gamma}}} \right) \dot{\boldsymbol{\gamma}}, & \tau \geq \tau_Y, \end{cases} \quad (4)$$

where K is the consistency, n the power-law index, τ_Y is the yield stress, and τ and $\dot{\boldsymbol{\gamma}}$ represent the second-invariants of the stress tensor and $\dot{\boldsymbol{\gamma}} \equiv \nabla \mathbf{u} + (\nabla \mathbf{u})^T$.

There is no slip on the wall of the slot or tube. At the left-hand inlet of the conduit, fluid is fed in with uniform speed V . At the right-hand outlet, “outflow” boundary conditions ($p = 0$ and $\partial \mathbf{u} / \partial x = \mathbf{0}$) are imposed. Inbetween, the flow field converges to a viscoplastic Poiseuille profile, which is interrupted by the bubble. At $t = 0$, the fluid inside the conduit is motionless and the bubble is set to have circular or hemispherical ends, buffering a uniform midsection with radius $0.9R$ and length $4R$; such bubbles are sufficiently long that the flow dynamics in steady state is insensitive to the precise initial shape. On the bubble interface, there is no tangential stress and the normal stress is balanced by interfacial tension (i.e. $\mathbf{n} \cdot \boldsymbol{\tau} \cdot \mathbf{n} - p = \sigma (\nabla \cdot \mathbf{n})$, where \mathbf{n} is the normal vector to the interface).

2.2. Computational details

We solve the governing equations numerically using the open source code Gerris. This scheme uses the volume-of-fluid method to deal with the interface of the bubble, introducing a concentration field $c(\mathbf{x}, t)$ that satisfies the scalar advection equation to track the interface and distinguish the viscoplastic fluid ($c = 1$) from the bubble ($c = 0$) [18]. The code also uses an adaptive spatial discretisation, providing high resolution along the interface and over the lubricating thin film [19]. Gerris does not account for the yield criterion of the viscoplastic fluid other than by a regularization strategy; we adopt the following revision of (4):

$$\tau_{jk} = \text{Min} \left(\mu + \frac{c\tau_Y}{\dot{\boldsymbol{\gamma}}}, \mu_{max} \right) \dot{\boldsymbol{\gamma}}_{jk}, \quad (5)$$

where μ_{max} is a viscous regularization parameter, along with the linear interpolations,

$$\rho = c\rho_1 + (1 - c)\rho_2 \quad \& \quad \mu = cK\dot{\boldsymbol{\gamma}}^{n-1} + (1 - c)\mu_2. \quad (6)$$

In practice, we use $R = 1$ m and a computational domain of length $17R$, which is large enough to allow the bubble to reach steady state as it propagates down the conduit and not be influenced by end effects. For the material parameters, we set $\sigma = 1$ N/m, $K = 0.03$ Pa s^{*n*}, $\rho_2 = \rho_1 = 1$ kg/m³, $\mu_{max} = 300$ Pa s and $\mu_2 = 0.03$ Pa s. We vary the inflow speed V , yield stress τ_Y and power-law index n to vary the Capillary number and rheology.

3. Lubrication analysis

To study the shallow film buffering the bubble from the adjacent wall, we use h_∞ as the characteristic lengthscale across the slot or tube, and $L = h_\infty C^{-1/3}$ as the scale along that conduit. For Herschel-Bulkley fluid, we define the Capillary number C in terms of a characteristic plastic viscosity $\mu = K(U/h_\infty)^{n-1}$. Given the dimensional cross-slot or radial position, r , and axial coordinate, z , we introduce a local dimensionless coordinate system (x, y) based on the wall such that

$$r = R - h_\infty y \quad \& \quad z = Lx, \quad (7)$$

and denote the dimensionless surface position by $y = h(x, t)$.

With $\epsilon \equiv h_\infty/L \equiv C^{1/3} \ll 1$, the usual lubrication analysis indicates that the pressure p is independent of y through the film. In

view of the normal stress condition at the interface, we then find the Laplace-Young relation,

$$p = -\frac{\sigma h_\infty}{L^2} \frac{h_{xx}}{(1 + \epsilon^2 h_x^2)^{3/2}} - \frac{\sigma}{R - h_\infty h} \approx -\frac{\sigma h_\infty}{L^2} h_{xx} - \frac{\sigma}{R}, \quad (8)$$

for the axisymmetric case and $p \approx -\sigma h_\infty L^{-2} h_{xx}$ for the planar problem. Here the subscript x is employed as a shorthand for derivative.

The lubrication theory also indicates that the shear stress (τ_{rz}) and $\partial u / \partial r$ dominate the other components of the stress and deformation rate tensors. The radial gradient of the shear stress must therefore balance the axial pressure gradient in the absence of inertia. One can then explicitly solve for the axial velocity field, $u(x, y, t)$:

$$u = \begin{cases} u_p [1 - (1 - y/Y)^{1+1/n}] & \text{if } 0 \leq y \leq Y, \\ u_p & \text{if } Y < y \leq h, \end{cases} \quad (9)$$

where

$$Y = \text{Max} \left(h - \frac{B}{|h_{xxx}|}, 0 \right) \quad (10)$$

is the surface dividing fully sheared fluid in $0 \leq y \leq Y$ from plug-like flow in $Y < y \leq h$, and

$$u_p = \frac{nY^{1+\frac{1}{n}} |h_{xxx}|^{\frac{1}{n}-1}}{(n+1)} h_{xxx} \quad \& \quad B = \frac{\tau_Y h_\infty}{\mu U} \quad (11)$$

are the plug speed and Bingham number. If $Y = 0$ in (10), $u_p = 0$ and the film is rigidly stuck to the tube wall.

In steady state, the fluid flux must be constant in the frame of the bubble (i.e. $2\pi R h_\infty \int_0^R (u - U) dy \approx \text{constant}$). Thus, after scaling,

$$1 = h - \frac{nY^{\frac{1}{n}+1} |h_{xxx}|^{\frac{1}{n}-1}}{(2n+1)(n+1)} [(2n+1)h - nY] h_{xxx}, \quad (12)$$

given that the film becomes flat, $h \rightarrow 1$ and $h_{xxx} \rightarrow 0$, away from the ends of the bubble.

3.1. At the front of the bubble

We now solve the preceding model in the frame of bubble using the travelling-wave coordinate $\xi = x - Ut$, and thereby match the residual wall layer to the meniscus at the front of the bubble. In terms of ξ , equations (10) and (12) can be combined into the algebraic-differential system,

$$h''' = \frac{B \text{sgn}(h-1)}{h-Y}, \quad (13)$$

$$\frac{nB^{\frac{1}{n}} Y^{\frac{1}{n}+1} [(2n+1)h - nY]}{(2n+1)(n+1)(h-Y)^{\frac{1}{n}}} = |h-1|, \quad (14)$$

as long as the film remains yielded (prime denoting derivative with respect to ξ).

For the front of the bubble, we may assume that $h''' > 0$ provided fluid is yielded. However, since $h = 1$ and $h''' = 0$ in the flat residual film for $\xi \rightarrow -\infty$, Y must vanish and the fluid become rigid at a finite yield position in ξ . To the left of this point, we abandon the system in (13) and (14) and set $h = 1$. The yield position, where $h \rightarrow 1$ and $Y \rightarrow 0$ from the right, can be shifted to $\xi = x - Ut = 0$ in view of the translational invariance. Thus, we may solve (13) and (14) only in $\xi > 0$, given suitable boundary conditions at $\xi = 0$.

At the yield position, $Y \rightarrow 0^+$ and so $h'''(0) = B$. The most obvious boundary conditions on the lower derivatives are that $h'(0) = h''(0) = 0$. This would certainly be the case if the constitutive law had been regularized in such a way that (10) was replaced by $Y = \text{Max}(\epsilon, h - B/h''')$, with $\epsilon \ll 1$. Then, continuity across $\xi = 0$,

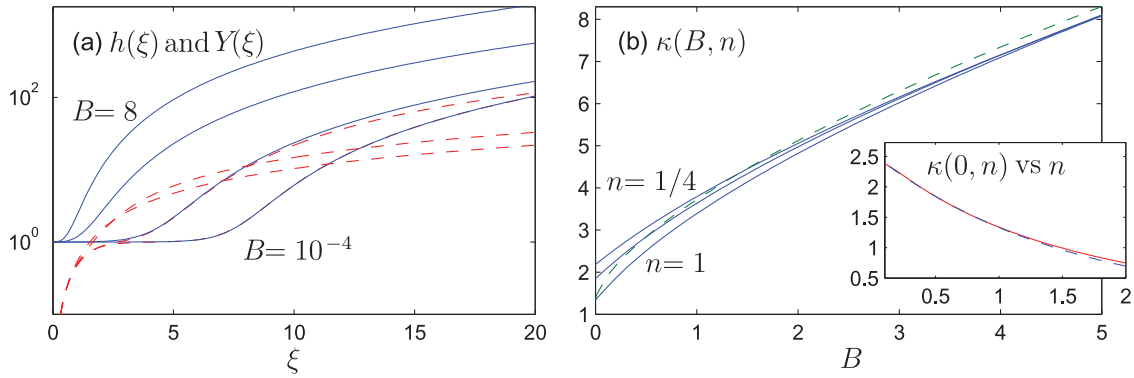


Fig. 1. (a) Solutions for a Bingham ($n = 1$) film near the front of the bubble for $B = 10^{-4}$, 0.01, 1 and 8. Shown are $h(\xi)$ (solid) and $Y(\xi)$ (dashed); h increases with B , whereas Y decreases with B at large ξ . (b) $h_{\xi\xi}(\xi \rightarrow \infty) = \kappa(B, n)$ versus B for $n = 1, \frac{1}{2}$ and $\frac{1}{4}$ (the data decrease with increasing n). The dashed line is the interpolant $\kappa(B, 1) \sim \kappa(0, 1) + 2.383B^{2/3}$; $\kappa(0, n)$ is plotted in the inset along with the approximation $2.553e^{-0.65n}$ (dashed line) [20]. Computations begin at $\xi = 0$ with $(h, h', h'') = (1 + B\delta^3/6, B\delta^2/2, B\delta)$ and $\delta = 10^{-5}$.

now defined as the location where $Y = \epsilon$, would demand that $h'(0)$ and $h''(0)$ vanish for $\epsilon \rightarrow 0$. Any other conditions on (h, h', h'') imply jumps on those quantities across the yield position and a singular capillary pressure that would force the yield position to move even had the constitutive model not been regularized.

We may now shoot away from $\xi = 0$ and compute the limiting curvature of the film for $\xi \rightarrow \infty$,

$$h_{\xi\xi}(\xi \rightarrow \infty) \equiv \kappa(B, n). \tag{15}$$

As argued by Bretherton, this curvature contributes a term to the total capillary pressure, $\sigma h_{\infty} L^{-2} h_{xx}$, that must match the corresponding term for a circular or hemispherical cap: $\sigma h_{\infty} L^{-2} h_{xx} \sim \sigma R^{-1}$. Thus,

$$\frac{h_{\infty}}{R} \sim C^{2/3} \kappa(B, n). \tag{16}$$

Fig. 1 (a) shows computations of the predicted film thickness $h(\xi)$ and boundary of the plug-like region $Y(\xi)$ with $n = 1$ and various values of B . For $B \ll 1$, Y converges to h except near the yield position and for very large ξ (since $h''' \rightarrow 0$ for $\xi \rightarrow \infty$, Y always diverges from h for sufficiently large ξ whatever the yield stress). For $B \gg 1$, Y becomes much less than h everywhere, signifying that the bulk of the film flows in a plug-like fashion. In this limit, $h''' \sim Bh^{-1}$. Thus $h = G(B^{1/3}\xi)$, where $GG'' = 1$.

Computations of $\kappa(B, n)$ are shown in Fig. 1(b). For $B \rightarrow 0$, this quantity limits to the matching constant expected for a power-law fluid which varies with n as plotted in the inset. For $B \gg 1$, on the other hand, $\kappa \sim 2.383B^{2/3}$, irrespective of n , given that $G'' \rightarrow 2.383$ for $B^{1/3}\xi \gg 1$. A simple interpolation formula that bridges between the two limits, and which works well for $n = 1$, is

$$\kappa(B, n) \sim \kappa(0, n) + 2.383B^{2/3}. \tag{17}$$

3.2. At the back of the bubble

We can also solve the lubrication model for the thickening of the viscoplastic film at the back of the bubble. In this instance, we can no longer assume that h''' remains of one sign. Indeed, as indicated by Bretherton, the Newtonian solution takes the form of a decaying oscillation (see also [21]). The situation corresponds to a viscoplastic contact line advancing into a pre-wetted film [22].

We now solve (13) and (14) subject to $h \rightarrow 1$ on the right and $h \rightarrow \frac{1}{2}\kappa\xi^2$ on the left, with κ determined by (15) which assures that the solution for the film at the back of the bubble corresponds to that matching the front meniscus. As illustrated by the numerical solution for $B = 1$ shown in Fig. 2(a), the solution accomplishes the decay to $h = 1$ by passing through an infinite sequence of switches in the sign of $h - 1$. This demands that h'' takes the

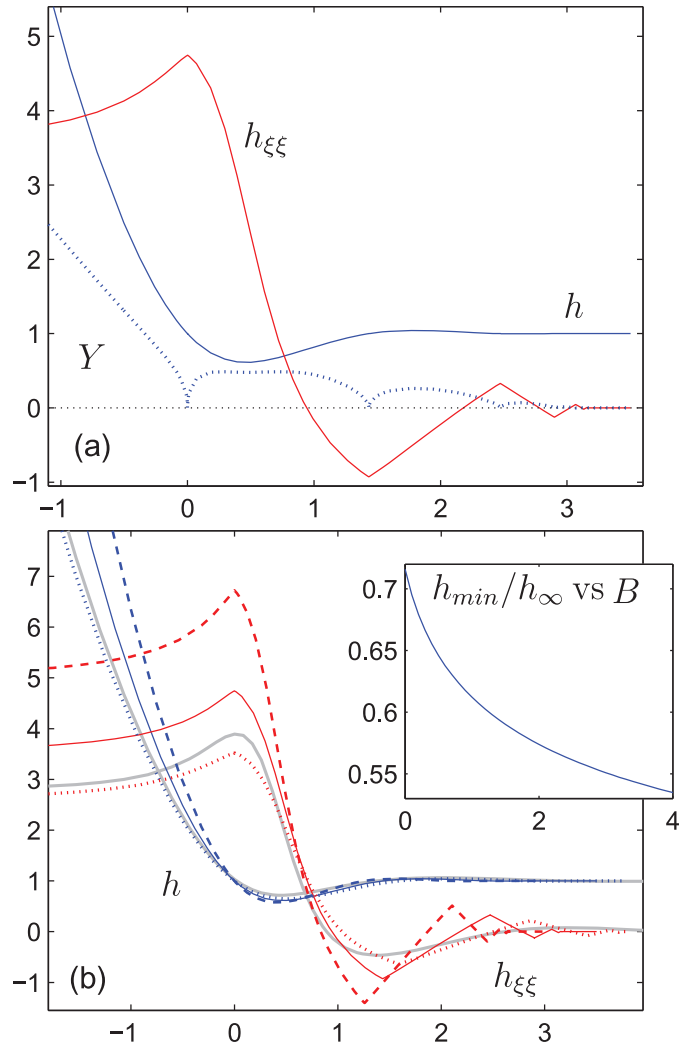


Fig. 2. (a) Lubrication solution for h, Y and h'' at the back of the bubble for $B = n = 1$. (b) Comparison of h and h'' for solutions with $B = 0$ (grey), $B = 1/2$ (dotted), $B = 1$ (solid) and $B = 2$ (dashed). The solutions are shifted in ξ so as to align the maxima in curvature. The inset of (b) shows the minimum film thickness relative to h_{∞} against B . The computations exploit a regularization parameter δ equivalent to that in (31): initially we set $\delta = 10^{-3}$ and a preliminary solution is computed; δ is then incrementally reduced to 10^{-8} by which point the solution converges to the viscoplastic limit.

form of a decaying sawtooth-like oscillation (with corners at the sign switches). Eventually, the oscillations satisfy the simpler problem $h''' \sim B \operatorname{sgn}(h - 1)$, indicating that the solution converges to a series of piecewise cubic polynomials. The oscillations decrease steadily in wavelength as well as amplitude (unlike the Newtonian film which has fixed wavelength), such that the series terminates after a finite distance, furnishing a finite yield position (Jalaal, Balmforth & Stoeber, *in preparation*).

Solutions with three different Bingham numbers are compared in Fig. 2(b). The decay to the flat film is faster for higher yield stress, with a deeper minimum in film thickness achieved relative to the residual limit h_∞ during the first oscillation in $h(\xi)$ (see the inset); the Newtonian value ($h_{\min} \approx 0.716h_\infty$) was quoted by Bretherton.

4. The film thickness

4.1. The leading-order residual film thickness

The result in (16) conceals the full dependence of the residual film thickness on the parameters of the problem because of our choice of dimensionless groups. In particular, both the Bingham number B and Capillary number C for $n \neq 1$ are defined above using h_∞ . Thus (16) is actually an implicit equation for the residual film thickness. If we define an alternative Capillary number based on tube radius,

$$\text{Ca} = \frac{KU^n}{\sigma R^{n-1}}, \tag{18}$$

then

$$\frac{h_\infty}{R} = \text{Ca}^{2/(2n+1)} [\kappa(B, n)]^{3/(2n+1)}, \tag{19}$$

which unravels the dependence of C on h_∞ , if not the Bingham number. If we go further and employ the interpolation in (17), we arrive at

$$\frac{(h_\infty/R)^{(2n+1)/3}}{\kappa(0, n) + 2.383 \text{Bi}^{2/3} (h_\infty/R)^{2n/3}} = \text{Ca}^{2/3}, \tag{20}$$

in terms of another Bingham number

$$\text{Bi} = \frac{\tau_Y R^n}{KU^n}. \tag{21}$$

The relation in (20) predicts that $h_\infty/R \sim 5.7 \text{Bi}^2 \text{Ca}^2$ when the yield stress term becomes dominant in the denominator, in agreement with dimensional analysis of plastic films [2].

In some other studies [10–12], h_∞ has been reported as a function of a different dimensionless group than our Capillary number. In particular, a group was employed based on the effective viscosity, $\mu + \tau_Y R/U$, rather than the plastic viscosity μ . The net effect of using this alternative dimensionless parameter is that, although the introduction of the yield stress at fixed Ca increases h_∞ , the residual wall thickness actually decreases for fixed $(\mu U + \tau_Y R)/\sigma \equiv \text{Ca}(1 + \text{Bi})$.¹

4.2. Corrected film thickness

Awkwardly, it is known (e.g. [23]) that the validity of Bretherton’s asymptotic solution for the Newtonian problem is limited to relatively low values of C (practically, $C < 0.01$). This limitation is restrictive when comparing predictions with numerical simulations and experiments. One way to improve the situation in a

non-asymptotic fashion is to retain the full surface curvature in the Laplace-Young relation [9,25–27]:

$$p = -\frac{\sigma h_\infty}{L^2} \mathcal{K}, \tag{22}$$

where

$$\mathcal{K} = \begin{cases} h_{xx}(1 + \epsilon^2 h_x^2)^{-3/2} & (\text{slot}), \\ h_{xx}(1 + \epsilon^2 h_x^2)^{-3/2} + (\mathcal{R} - \epsilon^2 h)^{-1} & (\text{tube}), \end{cases} \tag{23}$$

and

$$\mathcal{R} = \frac{R}{\epsilon^2 h_\infty}. \tag{24}$$

The rationale behind this inclusion is that the surface curvature can then be matched automatically into the meniscus region where surface gradients become arbitrarily large. As noted by Wilson [25], asymptotic justification can be provided by noticing that the additional terms that are thereby included constitute some of the next-order corrections in the lubrication theory, and those that, in particular, enter the leading-order relations over the meniscus.

We may further introduce a coordinate system based on the axial surface angle; i.e. $\theta = \tan^{-1}(\epsilon h_x)$. Writing now $h = h(\theta)$ and $\mathcal{K} = \mathcal{K}(\theta)$, we may turn the lubrication equations into the second-order problem,

$$\frac{dh}{d\theta} = \frac{\sin \theta}{\epsilon^2(\mathcal{K} - \Lambda)}, \quad \frac{d\mathcal{K}}{d\theta} = \frac{B \cos \theta}{\epsilon(\mathcal{K} - \Lambda)(h - Y)}, \tag{25}$$

where

$$\Lambda = \begin{cases} 0 & (\text{slot}), \\ \cos \theta / (\mathcal{R} - \epsilon^2 h) & (\text{tube}), \end{cases} \tag{26}$$

along with the algebraic relation in (14) and the boundary conditions

$$(h, \mathcal{K}) \rightarrow (1, 0) \text{ for } \theta \rightarrow 0 \tag{27}$$

and

$$h \rightarrow \epsilon^{-2} \mathcal{R} \text{ for } \theta \rightarrow \frac{1}{2}\pi. \tag{28}$$

The imposition of three boundary conditions fixes the parameter \mathcal{R} as an eigenvalue in addition to $h(\theta)$ and $\mathcal{K}(\theta)$. Given this solution, the axial position x corresponding to the local surface angle θ can be recovered by integrating

$$\frac{dx}{d\theta} = \frac{\cos \theta}{\epsilon(\mathcal{K} - \Lambda)}. \tag{29}$$

Computations of the residual wall thickness (now given by $h_\infty/R = \epsilon^2/\mathcal{R}$) for this “corrected model” are shown in Fig. 3. Results for both planar and axisymmetric bubbles are shown and compared with existing results for Newtonian fluids and our current computations with Gerris. The predictions are first plotted at fixed B against C , and then for fixed Bi_Q against Ca_Q , where

$$\text{Bi}_Q = \frac{\text{Bi}}{(1 - h_\infty/R)^j} \quad \& \quad \text{Ca}_Q = \text{Ca}(1 - h_\infty/R)^j,$$

where $j = 1$ or 2 for planar or axisymmetric geometry, respectively. Here, Bi_Q and Ca_Q are the Bingham and Capillary numbers defined in terms of the mean fluid speed $V = U(1 - h_\infty/R)^j$ (rather than bubble speed U), which are the more basic parameters in the Gerris computations.

The predictions of the corrected model in (25)–(29) match the existing Newtonian results and Gerris simulations for much higher residual film thicknesses than for the leading-order theory. However, there are still noticeable discrepancies between the lubrication analysis and Gerris simulations for Capillary numbers as low as 0.003 when the residual film thickness is of order 0.1 (by contrast, for Newtonian fluid, the corrected lubrication analysis performs well in comparison to computations upto Capillary numbers

¹ This is evident from Fig. 3, presented later, where one must translate each curve to the right by a factor $1 + \text{Bi}$, which easily swamps the trends plotted therein.

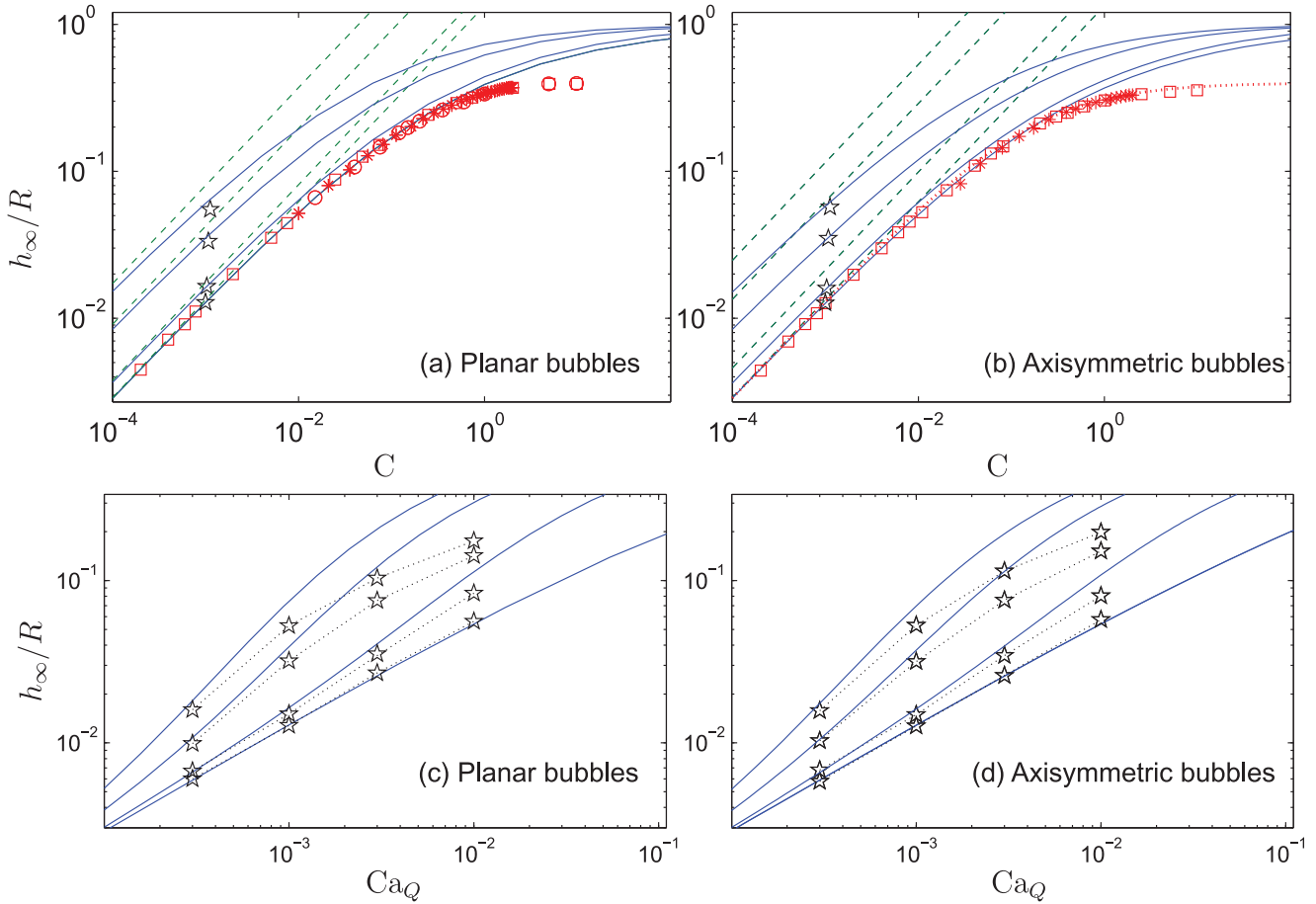


Fig. 3. Residual film thickness against C for (a) planar and (b) axisymmetric bubbles, for $B = 0, 0.16, 1.6$ and 5 ($n = 1$). Dashed lines show the leading-order prediction in (16); solid lines display the results of the model (25)–(29). The black pentagrams show results using Gerris. The (red) symbols indicate previous results from [23] (circles), [3] (stars) and [4] (squares). The dotted line in (b) is the so-called “Taylor law” [24]. In (c) and (d), the Gerris results and asymptotic predictions for fixed $Bi_Q = 10, 50$ and 100 are plotted against Ca_Q .

of order one [27]). We uncover a possible origin of this discrepancy below by looking in more detail at the flow field and bubble shape.

Before that, we conclude this section by showing results for power-law fluids, which have been studied previously in the current context both theoretically and experimentally [8,9,11]. Fig. 4 shows how the predictions of the corrected model for $n = 0.652$ compare well with Gerris simulations upto relatively high Capillary numbers. As noted previously by Soares et al. [11], the theoretical results are lower than measurements from the experiments of Kamisli & Ryan [8]. The latter match the Taylor law more closely for reasons that are not clear, but may have a rheological origin [11].

5. Bubble shapes and plugs

The corrected model of Section 4.2 can be rewritten to use arc length s (with scaling L) as the independent variable, which results in the system,

$$\frac{dx}{ds} = \cos \theta, \quad \frac{dh}{ds} = \epsilon^{-1} \sin \theta, \quad \frac{d\theta}{ds} = \epsilon(\mathcal{K} - \Lambda), \quad (30)$$

$$\frac{d\mathcal{K}}{ds} = \left[\frac{(2n+1)(n+1)|h-1|}{n[(2n+1)h-nY]h^{1+\frac{1}{n}}} \right]^n \frac{\cos \theta}{[\text{Max}(\delta, Y/h)]^{1+n}}, \quad (31)$$

along with (14) and (26). Imposing $(h, \theta) \rightarrow (\mathcal{R}/\epsilon^2, \pm \frac{1}{2}\pi)$ at the two end points then permits a computation of the entire bubble

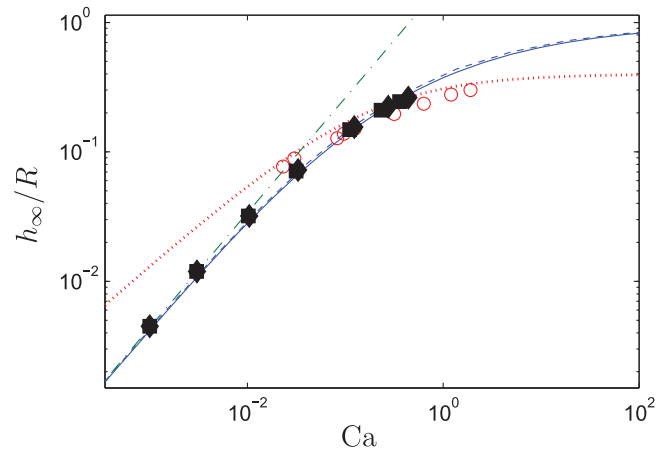


Fig. 4. Residual film thickness for power-law fluid with $n = 0.652$. The leading-order asymptotic result is shown by the dot-dashed line. The solid and dashed lines show the results of the corrected model (25)–(29) for axisymmetric and planar bubbles, respectively. The (almost overlapping) filled symbols show the Gerris results (diamonds for axisymmetric and squares for planar). The circles show experimental data taken from Kamisli & Ryan [8]. The dotted line shows the Taylor law.

including both the front and back menisci (and again treating \mathcal{R} as an eigenvalue; cf. [27]). To match a particular bubble volume, the total arc length must be suitably adjusted. The alternative form of (31) and inclusion of the regularization parameter δ eases the

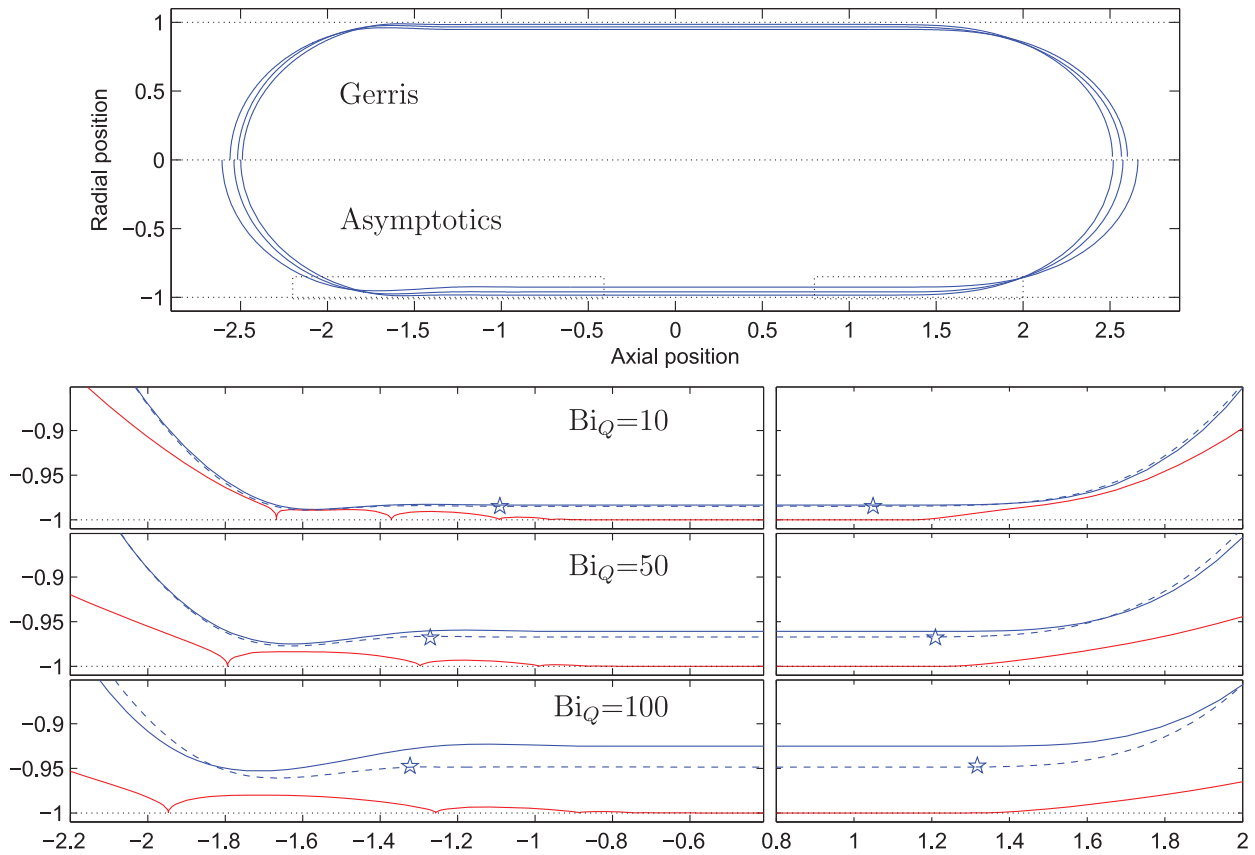


Fig. 5. Planar bubble shapes (in the frame of their center of mass) from the Gerris computations and predicted by the lubrication model in (30) and (31) for $Bi_Q = 10, 50$ and 100 , with $Ca_Q = 0.001$ and $n = 1$. The top panel compares the entire bubble profile (with Gerris solutions shown on top, asymptotic solutions below). The lower panels show magnifications of the back and front films, with the thickness h and yield surface Y of the asymptotics shown as solid lines and the Gerris bubble surface by dashed lines. The stars show the axial yield positions of the Gerris solutions, with the yield criterion defined according to where $\tau = \tau_\gamma$ for the regularized constitutive law.

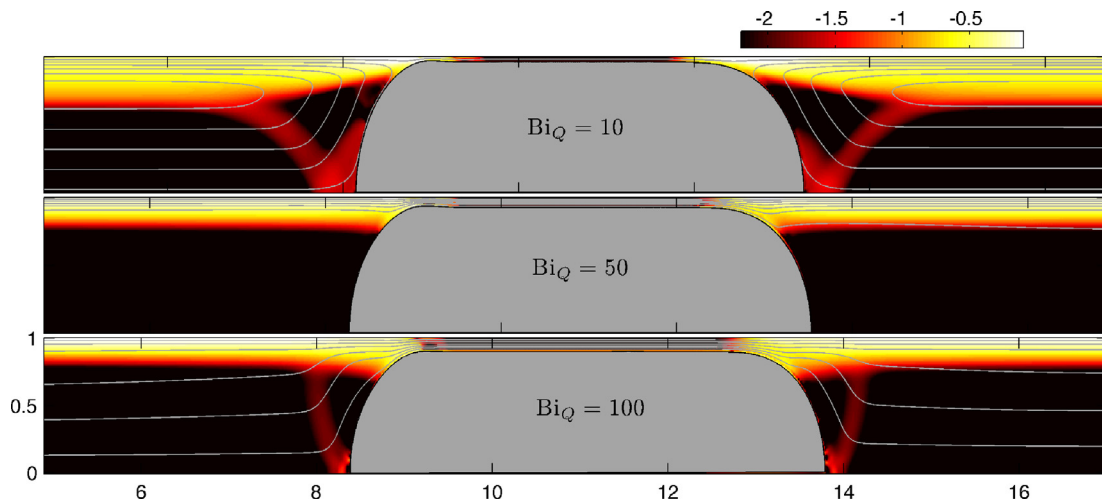


Fig. 6. Density maps of $\log_{10} \dot{\gamma}$ for $Ca_Q = 0.003$, $n = 1$ and $Bi_Q = 10, 50$ and 100 (top to bottom). Also shown are six streamlines (equally spaced in streamfunction) in the frame of reference of the bubble.

computations of the plugs, by first finding solutions for larger (though still small) values of δ , then continuing these solutions to the viscoplastic limit by incrementally reducing that parameter.

Fig. 5 compares the bubbles shapes predicted by (30) and (31) with the Gerris results for planar bubbles with $Ca_Q = 10^{-3}$ and three values of Bi_Q . For lower Bi_Q , the two agree qualitatively well, if not quantitatively, in the shape and thickness of the wall films and the yield position. For higher Bi_Q , however, the discrepancies are again visible.

More details of the flow fields from Gerris simulations for $Ca_Q = 0.003$ are shown in Fig. 6. The flow fields converge to the viscoplastic Poiseuille profiles upstream and downstream of the bubbles, complete with the central plugs. In the approach to the bubbles, the fluid yields and a more complicated pattern develops. For the case with lower yield stress ($Bi_Q = 10$), the streamline pattern is similar to that for the Newtonian problem in which fluid is recirculated up and downstream [4,28]; two off-axis regions of relatively low strain rate also develop near the bubble ends. For

the case with highest yield-stress, the streamline pattern is quite different, with flow being channelled entirely through the residual film ($Bi_Q = 100$; cf. [10,12]). Finally, for the case with intermediate yield stress ($Bi_Q = 50$), the plugs of the background flow continue almost to the bubble surfaces, leaving a narrow weakly yielded zone at the bubble ends that is difficult to discern in Fig. 6. Note that for special choices of the parameters, the bubble speed can match the speed of the plug in the background viscoplastic Poiseuille flow (see Appendix A), which allows the background plug to attach to the ends of the bubble. This attachment demands that the residual film thickness must become independent of Capillary number, which is not observed in Fig. 3. The background plugs cannot therefore be fully attached to the bubble except at the special parameter settings.

Overall, Fig. 6 illustrates how yield stresses in the vicinity of the ends of the bubble complicate the flow pattern and modify its structure from the Newtonian case. The solutions also hint that there may be localized plugs attached to the bubble (see the example with $Bi_Q = 10$), although the identification of such regions is obscured by our regularization of the constitutive law. Irrespective of such details, the flow patterns suggest that the disagreement between lubrication theory and Gerris simulations may originate from the growing impact of the yield stress near the ends of the bubble, as the asymptotic analysis predicts a relatively simple flow profile over those regions.

Note that the films buffering the bubble from the walls are always plugged in our computations. For thicker films, one can imagine that the bubble might break free of the wall, forcing the film to yield all along its length. At yet higher film thickness, one can then envision encapsulating the bubble within the plug of the background flow [29].

6. Concluding remarks

In this article we have provided a viscoplastic version of Bretherton's lubrication analysis of the thin films buffering a long bubble that is displaced down a slot or tube by ambient fluid flow. We have also provided complementary computations using the open source code Gerris. When the viscoplastic films are sufficiently thin, the lubrication predictions match the simulation results. However, when yield stresses are increased, those films thicken and the agreement is poorer. We have suggested that this discrepancy might be due to the growing impact of yield stresses on the flow pattern at the ends of the bubble.

Acknowledgement

MJ was the recipient of a Vannier scholarship during this work.

Appendix A. Attached plugs

If the bubble becomes attached to the central plug of the background viscoplastic Poiseuille flow, then we may immediately predict the residual film thickness: considering the Bingham case ($n = 1$), the position of the yield surface of the background flow relative to radius or width, $\eta = r_p/R$, is given by the solution to the algebraic equations,

$$Bi_Q = \frac{12\eta}{(3+2\eta+\eta^2)(1-\eta)^2} \quad \text{or} \quad \frac{6\eta}{(2+\eta)(1-\eta)^2}, \quad (\text{A.1})$$

for either the tube or channel. The plug speed is then

$$u_p = \frac{6V}{3+2\eta+\eta^2} \quad \text{or} \quad \frac{3V}{2+\eta}, \quad (\text{A.2})$$

if V is the mean flow speed. When the plug is attached, $u_p \equiv U = V/(1-h_\infty/R)^j$, and so

$$\frac{h_\infty}{R} = 1 - \sqrt{\frac{3+2\eta+\eta^2}{6}} \quad \text{or} \quad \frac{1}{3}(1-\eta). \quad (\text{A.3})$$

For large Bingham number, $\eta \approx 1 - \sqrt{2/Bi_Q}$, $u_p \approx V$ and $h_\infty \approx \frac{1}{3}R\sqrt{2/Bi_Q}$, for either geometry.

References

- [1] F.P. Bretherton, The motion of long bubbles in tubes, *J. Fluid Mech.* 10 (2) (1961) 166–188.
- [2] D. Quéré, Fluid coating on a fiber, *Annu. Rev. Fluid Mech.* 31 (1) (1999) 347–384.
- [3] D.A. Reinelt, P.G. Saffman, The penetration of a finger into a viscous fluid in a channel and tube, *SIAM J. Scientif. Stat. Comput.* 6 (3) (1985) 542–561.
- [4] M.D. Giavedoni, F.A. Saita, The axisymmetric and plane cases of a gas phase steadily displacing a Newtonian liquid: a simultaneous solution of the governing equations, *Phys. Fluids* 9 (8) (1997) 2420–2428.
- [5] J.S. Ro, G.M. Homsy, Viscoelastic free surface flows: thin film hydrodynamics of hele-shaw and dip coating flows, *J. Non-Newtonian Fluid Mech.* 57 (2) (1995) 203–225.
- [6] A. de Ryck, D. Quéré, Fluid coating from a polymer solution, *Langmuir* 14 (7) (1998) 1911–1914.
- [7] J. Ashmore, A.Q. Shen, H.P. Kavehpour, H.A. Stone, G.H. McKinley, Coating flows of non-Newtonian fluids: weakly and strongly elastic limits, *J. Eng. Math.* 60 (1) (2008) 17–41.
- [8] F. Kamisli, M.E. Ryan, Perturbation method in gas-assisted power-law fluid displacement in a circular tube and a rectangular channel, *Chem. Eng. J.* 75 (3) (1999) 167–176.
- [9] R.W. Hewson, N. Kapur, P.H. Gaskell, A model for film-forming with newtonian and shear-thinning fluids, *J. Non-Newtonian Fluid Mech.* 162 (1) (2009) 21–28.
- [10] D.A. de Sousa, E.J. Soares, R.S. de Queiroz, R.L. Thompson, Numerical investigation on gas-displacement of a shear-thinning liquid and a visco-plastic material in capillary tubes, *J. Non-Newtonian Fluid Mech.* 144 (2) (2007) 149–159.
- [11] E.J. Soares, M.S. Carvalho, P.R. de Souza Mendes, Gas-displacement of non-Newtonian liquids in capillary tubes, *Int. J. Heat Fluid Flow* 27 (1) (2006) 95–104.
- [12] R.L. Thompson, E.J. Soares, R.D.A. Bacchi, Further remarks on numerical investigation on gas displacement of a shear-thinning liquid and a visco-plastic material in capillary tubes, *J. Non-Newtonian Fluid Mech.* 165 (7) (2010) 448–452.
- [13] B. Laborie, F. Rouyer, D.E. Angelescu, E. Lorenceau, Yield-stress fluid deposition in circular channels, *J. Fluid Mech.* (2016).
- [14] M. Sweid, M. Moyers-Gonzalez, P. Wilson, C. Castelain, T. Burghelca, The landau-levich problem for a viscoplastic fluid, 21ème Congrès Français de Mécanique, Bordeaux (2013).
- [15] M. Maillard, J. Boujlel, P. Coussot, Flow characteristics around a plate withdrawn from a bath of yield stress fluid, *J. Non-Newtonian Fluid Mech.* 220 (2015) 33–43.
- [16] P. Zamankhan, B.T. Helenbrook, S. Takayama, J.B. Grotberg, Steady motion of Bingham liquid plugs in two-dimensional channels, *J. Fluid Mech.* 705 (2012) 258–279.
- [17] O.M. Lavrenteva, A. Nir, Viscoplastic flows with free boundaries and interfaces, *Rev. Chem. Eng.* 26 (5-6) (2010) 149–170.
- [18] S. Popinet, An accurate adaptive solver for surface-tension-driven interfacial flows, *J. Comput. Phys.* 228 (16) (2009) 5838–5866.
- [19] S. Popinet, Gerris: a tree-based adaptive solver for the incompressible euler equations in complex geometries, *J. Comput. Phys.* 190 (2) (2003) 572–600.
- [20] S.J. Weinstein, K.J. Ruschak, Coating flows, *Annu. Rev. Fluid Mech.* 36 (2004) 29–53.
- [21] E. Tuck, L. Schwartz, A numerical and asymptotic study of some third-order ordinary differential equations relevant to draining and coating flows, *SIAM Rev.* 32 (3) (1990) 453–469.
- [22] N.J. Balmforth, S. Ghadge, T. Myers, Surface tension driven fingering of a viscoplastic film, *J. Non-Newtonian Fluid Mech.* 142 (1) (2007) 143–149.
- [23] K. Ruschak, Boundary conditions at a liquid/air interface in lubrication flows, *J. Fluid Mech.* 119 (1982) 107–120.
- [24] P. Aussillous, D. Quéré, Quick deposition of a fluid on the wall of a tube, *Phys. Fluids* 12 (10) (2000) 2367–2371.
- [25] S.D. Wilson, The drag-out problem in film coating theory, *J. Eng. Math.* 16 (3) (1982) 209–221.
- [26] H. Khesghi, S. Kistler, L. Scriven, Rising and falling film flows: viewed from a first-order approximation, *Chem. Eng. Sci.* 47 (3) (1992) 683–694.
- [27] J. Ratulowski, H.-C. Chang, Transport of gas bubbles in capillaries, *Phys. Fluids A* 1 (10) (1989) 1642–1655.
- [28] M.D. Giavedoni, F.A. Saita, The rear meniscus of a long bubble steadily displacing a newtonian liquid in a capillary tube, *Phys. Fluids* 11 (1999) 786–794.
- [29] A. Maleki, S. Hormozi, A. Roustaei, I.A. Frigaard, Macro-size drop encapsulation, *J. Fluid Mech.* 769 (2015) 482–521.